

18 **Abstract**

19 Bimodal runoff behavior, characterized by two distinct peaks in flow response, often leads to
20 significant stormflow and associated flooding. Understanding and characterizing this phenomenon
21 is crucial for effective flood forecasting. However, this runoff behavior has been understudied and
22 poorly understood in semi-humid regions. In this study, we investigated the response
23 characteristics and occurrence conditions of bimodal hydrograph based on the hydrometric and
24 isotope data spanning 10 years in a semi-humid forested watershed in North China. The main
25 findings include: 1) the onset of the bimodal hydrograph exhibits a threshold behavior, with
26 delayed streamflow peaks occurring when the sum of event rainfall (P) and antecedent soil
27 moisture index prior to the rainfall (ASI) exceeds 200 mm; 2) isotopic hydrograph separation
28 reveals that delayed stormflow process is primarily driven by pre-event water, with increasing
29 contributions of pre-event water during catchment wetting-up; 3) the dynamic variation in
30 groundwater level precedes that of streamflow, establishing a hysteretic relationship wherein
31 groundwater level peaks before streamflow during delayed stormflow. These findings, supported
32 by onsite observations, emphasize the dominance of shallow groundwater flow in the generation
33 of delayed stormflow.

34 **Keywords:** Semi-humid watershed, Stormflow, Bimodal runoff response, Threshold, Shallow
35 groundwater

36 **1. Introduction**

37 Runoff generation is one of the most complex hydrological processes due to their complexity
38 and non-linearity (McDonnell *et al.*, 2007; McGuire & McDonnell, 2010; Phillips, 2003). At

39 different times of a year, the activation of different runoff generating mechanisms, and contrasting
40 compartments and flow routes form different hydrograph shapes, which are generally classified as
41 unimodal and bimodal response types (Jenkins *et al.*, 1994; Gu, 1996; Kosugi *et al.*, 2011). A
42 unimodal response is characterized by a needle-shaped peak which responds immediately to the
43 rainfall impulse. In contrast, the bimodal response contains a delayed damped arch-shaped peak
44 responding to the same rainfall impulse in addition to the direct peak (Martínez-Carreras *et al.*,
45 2016). Generally, the delayed peak in a bimodal event contributes substantially more runoff than
46 the first peak (Zillgens *et al.*, 2007). For instance, the study by Onda *et al.* (2001) showed that the
47 delayed peak discharge is five to ten times greater than the first peak. When the bimodal runoff
48 event occurs, the streamflow increases markedly and lasts for several days. Therefore,
49 characterizing the bimodal response is of great significance to understanding the runoff generation
50 process and essential to achieving improved forecasting of extreme floods.

51 Since the bimodal hydrograph was accidentally observed in Côte d'Ivoire in 1960 during flood
52 frequency analysis and surface runoff generation study (Dubreuil, 1960, 1985), bimodal response
53 has piqued the interest of many hydrologists worldwide and been recorded in watersheds with
54 varied geological and climate conditions. For example, Onda *et al.* (2001) observed bimodal
55 hydrographs in a steep mountainous watershed underlain by shale and serpentinite in Japan (annual
56 precipitation: 1800 mm). Padilla *et al.* (2014, 2015) found delayed peaks after the rainfall in a
57 steep headwater catchment underlain by fractured bedrock also in Japan (annual precipitation:
58 2669 mm). Zillgens *et al.* (2007) recorded a delayed peak after the direct peak in Saalach basin in
59 the Austrian Alps (annual precipitation: 1400 mm). Masiyandima *et al.* (2003) found bimodal
60 responses in an inland valley watershed with wet lowlands in central Côte d'Ivoire (annual rainfall:
61 1045 mm). Anderson and Burt (1977, 1978) observed delayed peak after the storm at Bicknoller

62 Combe in Sommerset, composed of impermeable Old Red Sandstone. The characteristics and
63 conditions of occurrence of bimodal hydrograph can provide an effective method for simplifying
64 the description of complex hydrological systems, and comparing stormflow generation mechanism
65 in different watersheds (Tromp-van Meerveld & McDonnel, 2006). However, most of these studies
66 mentioned above have been done in humid regions with rainfall of more than 1000 mm. To the
67 best of authors' knowledge, very few studies if not none have been conducted in semi-humid
68 environment with rainfall less than 800 mm.

69 Meanwhile, recognizing the pivotal role of bimodal response in runoff generation, researchers
70 have made concerted efforts over the past several decades to quantify its characteristics and
71 establish statistical metrics for identifying the occurrence of bimodal events. Findings suggest that
72 indicators for bimodal response encompass factors such as rainfall amount (Haga *et al.*, 2005),
73 pre-event streamflow (Graeff *et al.*, 2009), soil moisture (Anderson & Burt, 1978; Weyman, 1970),
74 groundwater level (Padilla *et al.*, 2015) and storage (Martínez-Carreras *et al.*, 2016). Taking the
75 work of Martínez-Carreras *et al.* (2016) as an illustrative example, it revealed that the delayed peak
76 manifested only when the watershed storage reached a critical threshold of 113 mm. It is
77 noteworthy that predictors vary significantly among watersheds, with only a limited number of
78 studies presenting quantitative results akin to those reported by Martínez-Carreras *et al.* (2016).
79 Moreover, response timing metrics such as response lag to peak—providing insights into different
80 aspects of water travel time during an event—have received comparatively less attention in the
81 evaluation of threshold effects (Dingman, 2015; Ross *et al.*, 2021).

82 Many studies have delved into the compartments and flow pathways responsible for
83 generating distinct runoff response patterns. The first runoff peaks are attributed to factors such as
84 rainwater directly falling onto the stream channel, rapid flow through preferential paths (Becker

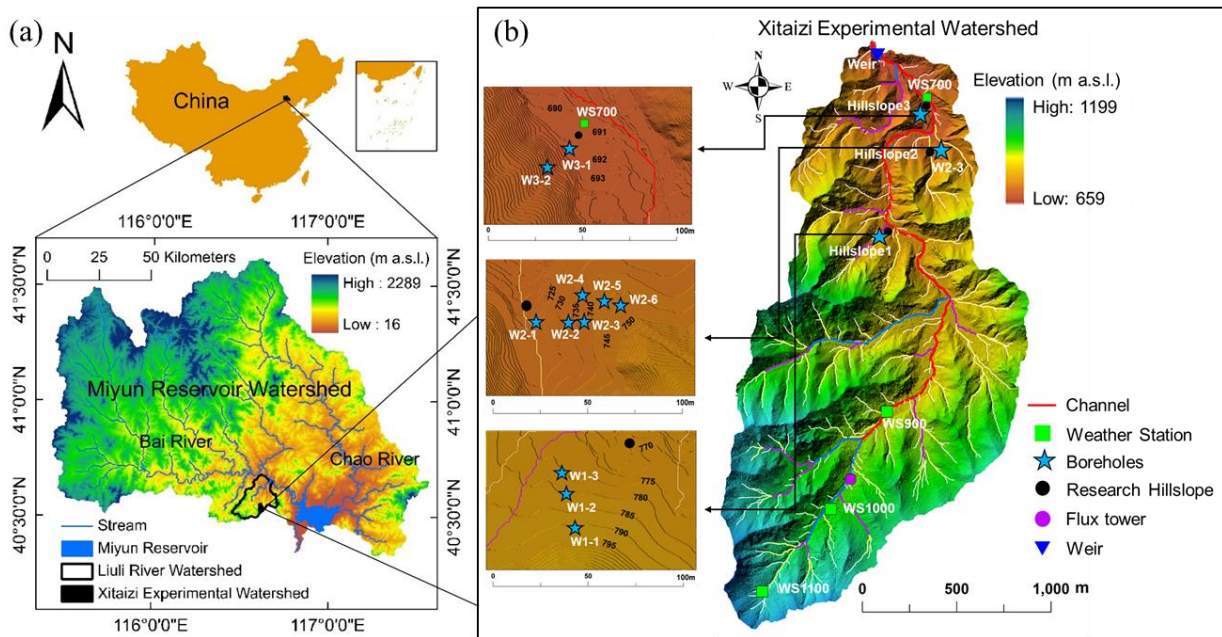
85 & McDonnell, 1998; Martínez-Carreras *et al.*, 2015; Wrede *et al.*, 2015), or saturation-excess
86 overland flow in the riparian zone (Anderson & Burt, 1978; Westhoff *et al.*, 2011). While delayed
87 runoff peaks in bimodal events are primarily linked to subsurface flow processes (Weyman, 1970;
88 Onda *et al.*, 2006; Zillgens *et al.*, 2007; Graeff *et al.*, 2009; Padilla *et al.*, 2015). However, a notable
89 gap exists in the literature, as many studies have focused solely on water flow processes within the
90 soil profile without thoroughly investigating whether subsurface stormflow originates from the
91 soil layer, bedrock layer, or a combination of both.

92 Bimodal responses, representing the nonlinear interplay between runoff and rainfall,
93 inherently showcase the stormflow process in terms of both response timing and magnitude. This
94 intuitive manifestation holds significant implications for advancing runoff modeling (Graeff *et al.*,
95 2009; McDonnell *et al.*, 2007) and enhancing the precision of flash flood forecasting (Zhang *et al.*,
96 2021; Zillgens *et al.*, 2007). In our present study, spanning the years 2014 to 2023, we collected
97 data on rainfall, groundwater levels, soil water content, and streamflow within a semi-humid forest
98 experimental watershed in North China. Our investigation involves characterizing the response
99 magnitude and timing of stormflow to rainfall through hydrograph analysis, while also scrutinizing
100 the composition of the water sources contributing to stormflow. Specifically, we hypothesize that
101 (1) the occurrence of bimodal streamflow responses exhibits a threshold behavior with rainfall and
102 watershed wetness, and (2) the primary source of water for the delayed stormflow is subsurface
103 flow.

104 **2. Materials and Methods**

105 **2.1 Study area**

106 The study headwater catchment, the Xitaizi Experimental Watershed (XEW), is situated at
107 coordinates 40°32'N and 116°37'E, as depicted in Fig. 1. Spanning an area of 4.22 km², XEW
108 exhibits elevations ranging from 676 to 1201 m above sea level. Approximately 54% of the area
109 features a slope between 20% and 40%. The region experiences a monsoon-influenced semi-humid
110 climate characterized by an average annual rainfall of 625 mm. The majority of this precipitation,
111 around 80%, occurs between June and September. The annual mean temperature in the area is
112 11.5°C, accompanied by a relative humidity of 59.1%. Experimental and observational activities
113 were conducted over the period from 2014 to 2023.



114 **Figure 1.** Location of the Xitaizi Experimental Watershed (XEW) in North China (a), and the
115 detailed distributed monitoring stations and instruments (b), including four automatic weather
116 stations (WS700-1100), one weir, and eleven groundwater boreholes (blue star corresponds with
117 well numbers and locations). Four rain gauges are located near the weather stations, and one is
118 located adjacent to the weir.
119

120

121 XEW represents a typical location in North China's earth-rocky mountainous region, where
122 approximately 80% of the catchment area is underlain by firmly compacted, deeply weathered
123 granite. Soil mapping and field investigations reveal the prevalent soil types to be brown earth and
124 cinnamon soil (according to Chinese soil taxonomy), with a depth extending to 1.5 meters. The
125 saturated hydraulic conductivity of the soil ranges from 19.5 to 175.3 mm/h, with an average value
126 of 45 mm/h. The bedrock in the area is primarily composed of granite, constituting approximately
127 88% of the total bedrock composition, while gneiss and dolomite are sporadically distributed.
128 Some sections of the granite exhibit fracture, and a layer of regolith is sandwiched between the
129 soil layer and the bedrock layer. In terms of land cover, the catchment is predominantly covered
130 by forest (98%), with 54.2% being broad-leaved, 2.3% coniferous, and 10.5% a mix of coniferous
131 and broad-leaved. The remaining 33% consists of shrubs (Tie *et al.*, 2017).

132 **2.2 Meteorology and runoff measurements**

133 Meteorological variables and runoff have been systematically monitored since 2013.
134 Meteorological conditions were consistently measured using four GRWS100 automatic weather
135 stations. These weather stations were strategically distributed quasi-uniformly along the elevation
136 gradient, as depicted in Fig. 1. The comprehensive data collection from these stations contributes
137 to a thorough understanding of the meteorological dynamics in the study area over the specified
138 timeframe.

139 For the measurement of air temperature (T_a) and relative humidity at each automatic weather
140 station, an HC2S3-L temperature and relative humidity probe was utilized. These probes were
141 equipped with a radiation shield to enhance accuracy. Simultaneously, a LI-190R quantum sensor
142 was employed to measure photosynthetically active radiation (PAR). Rainfall data were collected
143 at 10-minute intervals using six tipping-bucket rain gauges. These gauges were positioned in an

144 open space near the automatic weather stations, and average values were adopted for analysis in
145 this study.

146 Furthermore, the antecedent precipitation index (API), generally used to represent the residual
147 effect of previous precipitation (Mosley, 1979; Iwagami *et al.*, 2010), was calculated for all the
148 events over 3, 6, and 12 days. The API during the antecedent t days is described as follows:

$$149 \quad \text{API}(t) = \sum_{i=1}^t \frac{P_i}{i} \quad (1)$$

150 where i is the day count and P_i is the daily precipitation in the i^{th} day previously.

151 A Parshall flume was installed at the catchment outlet to measure streamflow (Fig. 1). The
152 water level in the flume was measured every 5 min with a HOBO capacitance water level logger
153 from 2014. Streamflow was calculated using the standard Parshall flume rating curve, and both
154 the rainfall and streamflow measurements were averaged to hourly timesteps, and in this study,
155 the analysis is conducted at hourly timesteps. Unfortunately, the observation equipment is
156 susceptible to failures due to the complex environmental conditions and disturbances caused by
157 wild animals and plants. Compounded by the remote location of XEW, accessing the site promptly
158 to address malfunctions is challenging, leading to the loss of some observation data. Notably,
159 stormflow data from July 19 to August 16, 2016, had to be excluded because the road collapsed
160 during a heavy storm, preventing a significant amount of runoff from passing through the Parshall
161 flume. Furthermore, streamflow data from 2018 to 2019 are unavailable, and the two bimodal
162 events in 2016 were omitted from the hysteresis analysis due to substantial errors in streamflow
163 observations resulting from damage to the diversion channel. The specific observation periods are
164 detailed in Table 1. These limitations underscore the challenges associated with conducting
165 observations in remote and environmentally intricate locations.

166 **Table 1.** Rainfall-runoff event classification and counts by year. This table provides a
 167 breakdown of the number of rainfall-runoff events categorized as unimodal, bimodal, and hybrid
 168 bimodal for each year, along with the corresponding time periods. The total counts are
 169 summarized at the bottom.

Year	Unimodal event	Bimodal event	Hybrid bimodal event	Time period
Characteristics	A needle-shaped peak which responds immediately to the rainfall impulse	A delayed damped arch-shaped peak responding to the same rainfall impulse in addition to the direct peak	The delayed peak increased rapidly and merged with the direct peak, generating extremely high streamflow volume	
2014	7	-	-	Jul 25 - Sep 25
2015	12	2	-	Jun 1 - Oct 1
2016	2	2	1	Jul 10 - Aug 20
2017	-	2	-	Jun 20 - Jul 10
2020	14	2	-	Jul 1 - Oct 10
2021	15	5	2	Jun1 - Oct 10
2022	18	1	-	Apr 1 - Nov 1
2023	9	-	1	Apr 1 - Nov 1
Total	77	14	4	

170

171 **2.3. Soil water content observation**

172 Volumetric soil water content (SWC) was measured at eight observation sites using CS616
 173 time-domain reflectometry (TDR) probes at 10-min intervals. On Hillslope 1, five soil moisture
 174 sensors were deployed, with an additional three located adjacent to WS900. These sensors were
 175 strategically placed in the soil profiles at 80 cm depth intervals, each at a depth of 10 cm. For
 176 analysis in this study, the 10-minute interval measurements were aggregated to hourly time steps,
 177 and the arithmetic mean of the total SWC across the four profiles was employed. Moreover, SWC
 178 data immediately preceding a rainfall event were integrated over the 80 cm depth to calculate an
 179 antecedent soil moisture index (ASI), as proposed by Haga *et al.* (2005). This index, commonly
 180 utilized in analyzing the impact of antecedent shallow soil water storage on catchment runoff

181 response (Fu *et al.*, 2013; Penna *et al.*, 2011), provides valuable insights into the soil moisture
182 conditions preceding rainfall events.

183 **2.4 Groundwater level observation**

184 Fluctuations in groundwater level (below the ground surface, hereinafter referred to as bgs)
185 were systematically recorded in eleven 80 mm diameter boreholes situated on three hillslopes
186 within the catchment (refer to Fig. 1). The boreholes were drilled to depths of 5-26 m in granite
187 (weathered and fractured to varying extents) mantled by thin soils. Unscreened portions of the
188 boreholes accounted for approximately one third to three fifths of the total depth (refer to Table 2).
189 To capture the groundwater level dynamics, HOBO capacitance water level loggers (Onset, USA)
190 were deployed to record water levels in the boreholes at hourly intervals. It is noteworthy that
191 water levels were rarely observed in boreholes W1-1, W1-2, W2-4, W2-5, and W2-6. This
192 observation could be attributed to the boreholes potentially not being drilled deep enough to reach
193 the groundwater, possibly due to challenges encountered during field drilling. Slug tests conducted
194 following installation suggested that the saturated conductivity in the weathered and fractured
195 granite was relatively high, ranging from 5.2×10^{-3} m/day to as high as 1.16 m/day.

196

197

198

199

200

201

202 **Table 2.** Depths and groundwater levels of boreholes. This table summarizes the depths of the
 203 bottom and the boundary between unscreened and screened portions, along with the shallowest
 204 and deepest groundwater levels of boreholes in the study area.

Borehole	Bottom (m)	Boundary (m)	Shallowest GWL (m)	Deepest GWL (m)
W1-3	10	6	2.8	10 ^a
W2-1	5	2	0.2	2.2
W2-2	10	4	4.8	10 ^a
W2-3	26	9	6.4	12.2
W3-1	10	4	0.8	3.9
W3-2	10	4	6.1	9.9

205 Note: All values indicate depths (in meters) from the ground surface; GWL represents groundwater
 206 level; 'a' indicates the groundwater level dropped below the bottom of the borehole.

207
 208 An index for groundwater level (I_G) was computed by normalizing the groundwater levels in
 209 each borehole to their recorded range throughout the research years, following the approach
 210 outlined by Detty and McGuire (2010). Subsequently, the arithmetic mean of I_G across all
 211 boreholes was calculated, serving as a representative proxy for the groundwater level across the
 212 entire catchment. This approach provides a standardized measure that allows for the comparison
 213 of groundwater level variations across different boreholes within the study area.

214 **2.5 Separation of rainfall-runoff events**

215 An intensity-based automatic algorithm, as outlined by Tian *et al.* (2012) and Powell *et al.*
 216 (2007), was employed to delineate and segregate rainfall events from hourly rainfall time series
 217 data. In this algorithm, a threshold rainfall intensity of >0.1 mm/h was utilized to determine the
 218 commencement and conclusion of each event, with individual storms being separated by a
 219 minimum of six hours. Events characterized by an accumulated rainfall exceeding 5 mm were
 220 selected for further analysis. A total of 95 distinct rainfall events, each with a cumulative rainfall
 221 of at least 5 mm, were identified and isolated from the rainfall data series spanning the years 2014
 222 to 2023, employing the intensity-based automatic method (refer to Table 1).

223 Storm runoff events are identified when streamflow experiences a rapid increase and attains
224 a peak in response to a rain impulse. Throughout the analyses presented, streamflow refers to the
225 total discharge measured at the weir. The computer program HYSEP (Sloto & Crouse, 1996) was
226 employed to automatically partition a streamflow hydrograph into baseflow and stormflow
227 components. Subsequently, the automated separation outcomes underwent manual verification and
228 adjustment, aligning with observed data and widely accepted straight-line separation principles. In
229 the context of each event, q_0 is defined as the streamflow before the onset of rainfall. This
230 parameter characterizes the baseflow conditions preceding the hydrograph's response to a rain
231 impulse (Zillgens *et al.*, 2007). The separation of stormflow from base flow allows for a more
232 detailed examination of the runoff dynamics during distinct rainfall events.

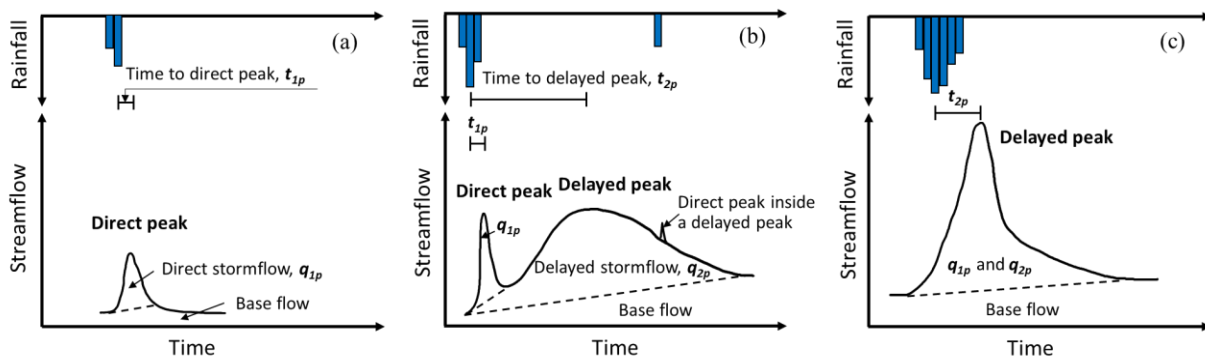
233 **2.6 Hydrograph and event types**

234 The hydrograph served as a valuable tool for characterizing the timing, magnitude, and
235 duration of runoff responses to rainfall. Three primary response types were identified based on the
236 number and shape of streamflow peaks: unimodal, bimodal and hybrid bimodal events. Schematic
237 diagrams illustrating these three types of events are presented in Fig. 2.

238 A unimodal event has a single peak generates during or shortly after the cessation of rain
239 impulse (refer to Fig. 2a). While a bimodal event features two peaks as a response to the same rain
240 impulse, of which the direct peak (also called the first peak) corresponds to a fast catchment
241 response to rainfall and occurs synchronously with the rainfall or shortly after its onset.
242 Additionally, we referred those events has a similarly shaped hydrograph to unimodal event, but
243 the water yield and peak delay time are significantly greater, as hybrid bimodal events. Hybrid
244 bimodal events can be distinguished from unimodal events by their extremely high streamflow

245 volume, longer duration, and delayed response time (Fig. 2c). The hydrographs of bimodal and
 246 hybrid bimodal events can refer to Fig. 12.

247 It's worth noting that a rainfall event may consist of multiple impulses, and in such cases, the
 248 hydrograph responds with multiple direct peaks (see Fig. 2b). The stormflows from the first peak
 249 (q_{1p}) and delayed peak (q_{2p}), along with the total event stormflow ($q_s = q_{1p} + q_{2p}$), were calculated
 250 by summing hourly values over the identified event period. The runoff ratio (Rr), commonly used
 251 to estimate the effective contributing area during a runoff event (Buttle *et al.*, 2004; Detty &
 252 McGuire, 2010), is calculated as the ratio of q_s to gross rainfall.



253
 254 **Figure 2.** Schematic diagrams of the hydrographs of an (a) unimodal event, (b) typical bimodal
 255 events, and (c) hybrid bimodal event.

256

257 2.7 Definition of lag time

258 The lag time, defined as the duration between peak rainfall and peak streamflow (Mosley,
 259 1979), is a critical parameter for modeling the temporal variability of streamflow. Lag time varies
 260 significantly among different water sources (Becker, 2005; Haga *et al.*, 2005) and has been
 261 introduced to comprehend sub-components of runoff in different response processes. In this study,
 262 two specific lag times are considered: t_{1p} the time lag between peak rainfall intensity and the first

263 streamflow peak, and t_{2p} the time lag between peak rainfall intensity and the delayed streamflow
264 peak, as illustrated in Fig. 2.

265 **2.8 Water sampling and isotope analysis**

266 Water samples for isotope analysis ($\delta^{18}\text{O}$ and δD) were collected from July 1 to September 1,
267 2021. Rainwater was automatically sampled every two hours using an ISCO6712 automatic water
268 sampler (Inc., Lincoln, Nebraska, USA) positioned near the weir. Manual bulk samples of rainfall
269 were also collected at the same location after each event using a rainwater sampler with a 9.5 cm
270 diameter funnel attached to a 500 ml plastic water bottle, insulated with bubble foil to protect
271 against direct sunlight, and a table tennis ball placed in the funnel's mouth to minimize evaporation.

272 Stream water was collected every two hours upstream of the Parshall flume location using an
273 automatic water sampler (Fig. 1). Spring, seepage water, and groundwater were manually collected
274 daily from boreholes using a bailer. All collected samples underwent isotopic composition analysis
275 ($\delta^{18}\text{O}$ and δD) using a Picarro L2140-i isotopic liquid water and water vapor analyzer (wavelength-
276 scanned cavity ring-down spectroscopy, WS-CRDS) with a declared precision of $\delta^{18}\text{O} \pm 0.1\text{‰}$ and
277 $\delta\text{D} \pm 1\text{‰}$.

278 **2.9 Isotopic hydrograph separation**

279 To trace the source of the streamflow during storm events, a simple mass balance approach
280 was employed to segregate the streamflow into two components: event water and pre-event water.
281 These components are represented by rainfall and baseflow, respectively, based on the oxygen
282 isotopic concentration ($\delta^{18}\text{O}$) of each component. The $\delta^{18}\text{O}$ of baseflow and weighted rainwater
283 samples served as end members, defining the ultimate isotopic composition of the stream, in
284 accordance with the approach outlined by Padilla *et al.* (2014):

$$285 \quad C_s = xC_e + (1 - x)C_p \quad (2)$$

286

$$x = \frac{C_s - C_p}{C_e - C_p} \cdot 100[\%] \quad (3)$$

287

where C_s , C_e and C_p refer to $\delta^{18}\text{O}$ concentrations of stream, event and pre-event water components,

288

respectively. C_e is the weighted value calculated using the incremental mean weighting method

289

(McDonnell *et al.*, 1990) for each event. C_p is determined from the stream $\delta^{18}\text{O}$ concentration

290

measured immediately preceding the rainfall. x is the percentage of event water in stream.

291

3. Results

292

3.1 Characteristics of different runoff response types

293

During the period from 2014 to 2023, a total of 95 distinct rainfall events, each with a

294

cumulative rainfall of at least 5 mm, were identified from the rainfall data series. Among these

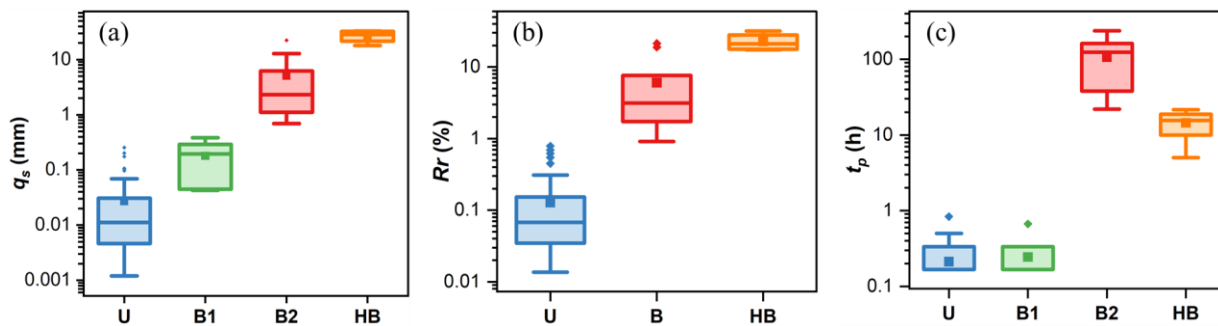
295

events, 14 exhibited a bimodal response, and an additional 4 displayed a hybrid bimodal process

296

(refer to Table 1).

297



298

Figure 3. Comparison of (a) stormflow, q_s , (b) runoff ratio, Rr and (c) lag time (t_p) from peak

299

rainfall to peak streamflow of different event types. U indicates unimodal event, B (including the

300

first peak B1 and the delayed peak B2) bimodal event and HB hybrid bimodal event. In each

301

boxplot, the lower and upper limits represent the lower and upper quartiles, while the whiskers

302

extend to the minimum and maximum values in each dataset. The horizontal line within the box

303

signifies the median. Individual asterisks denote points more than 1.5 times away from the median.

304

It's noteworthy that a semi-logarithmic coordinate was utilized for enhanced interpretability due

305

to the extensive range.

306

307 The stormflow volume and lag times of streamflow peaks for both unimodal and bimodal
308 events were determined and characterized. As depicted in Fig. 3, unimodal events generated
309 relatively minimal runoff, with a maximum q_{1p} of 0.25 mm. In contrast, the q_{1p} and q_{2p} of bimodal
310 events exhibited a wider range, spanning from 0.03 to 0.38 mm and from 0.82 to 31.63 mm,
311 respectively (Fig. 3b). The stormflow volume of bimodal events proved to be 3 to 114 times larger
312 than that of unimodal events, primarily due to the presence of delayed peaks (Fig. 3a).
313 Correspondingly, bimodal events displayed higher Rr values ranging from 0.91% to 31.81%,
314 whereas the Rr of unimodal events remained below 0.8% (Fig. 3b). This discrepancy suggests an
315 expanded effective contributing area during bimodal and hybrid bimodal events, as highlighted in
316 previous studies (Zhang *et al.*, 2021).

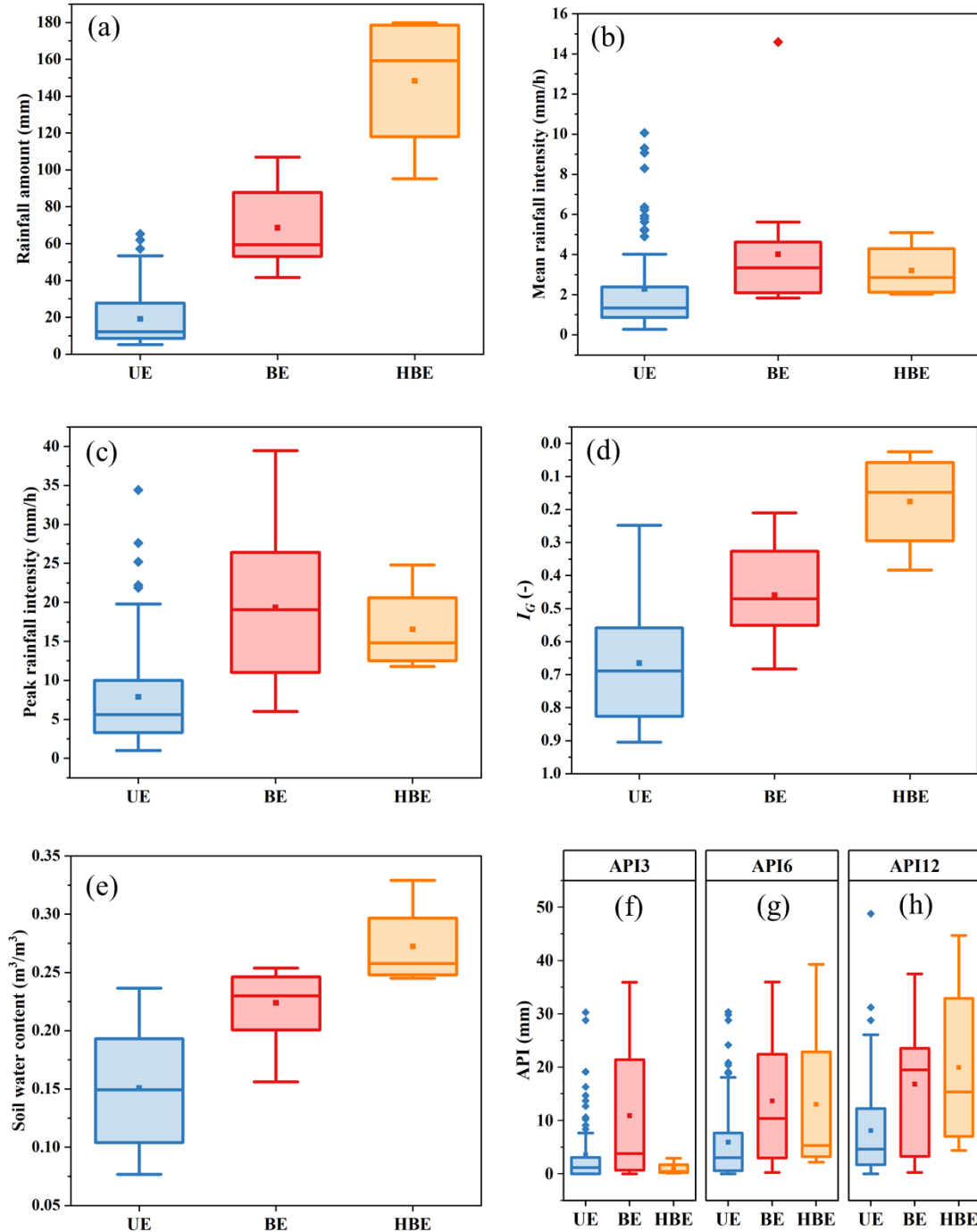
317 In both unimodal and bimodal events, all direct peaks were observed within a one-hour
318 timeframe. However, the delayed peak, a distinctive feature of bimodal events, manifested itself
319 between 5 hours and 9.9 days after the occurrence of the direct peak. Notably, hybrid bimodal
320 events exhibited shorter lag times and significantly higher stormflow yield, underscoring the need
321 for heightened attention in flood forecasting. The substantial difference in lag time strongly implies
322 that these peaks are contributed by distinct water sources, aligning with findings from previous
323 studies (Haga *et al.*, 2005).

324 **3.2 Determinants of delayed streamflow peaks**

325 The relationships between different event types and rainfall characteristic parameters and
326 watershed wetness indicators were further depicted in Fig. 4. It is noteworthy that the soil water
327 content (SWC) and groundwater level index (I_G) presented in Fig. 4 represent data recorded at the
328 end of rainfall events, considering that delayed streamflow peaks typically manifest subsequent to
329 the cessation of rainfall events. Rainfall amount, I_G , and SWC were statistically significantly

330 different for both groups, as proven by the t-test of equality of medians at a significance level of
331 $\alpha=0.01$. The transition from unimodal to bimodal events reveals a consistent increase in rainfall
332 amount, I_G , and SWC. Nearly all bimodal events exhibited rainfall amounts exceeding 50 mm,
333 whereas the range for unimodal events varied from 5.2 to 66.6 mm (Fig. 4a). This suggests that
334 the initiation of delayed streamflow peaks may be associated with substantial rainfall.

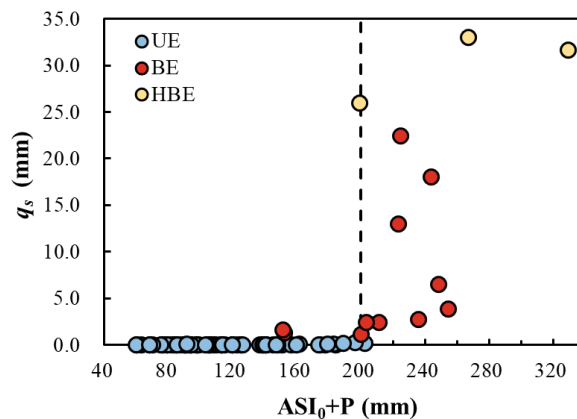
335 The I_G and SWC of bimodal events, especially hybrid bimodal events, were significantly
336 higher ($p < 0.01$) than those of unimodal events. Despite partial overlap in the ranges of I_G and
337 SWC for these groups (Fig. 4d and e), the mean I_G and SWC values for bimodal events (0.46 and
338 0.67) were notably greater than those for unimodal events (0.22 and 0.13), underscoring the
339 distinctiveness of these parameters between event types. Contrastingly, peak rainfall intensity,
340 mean rainfall intensity, and Antecedent Precipitation Index (API) metrics (API3, API6, and API12)
341 exhibited a widespread overlap in their variation ($p > 0.05$, Fig. 4b, d, g-i). Consequently, while
342 bimodal events were characterized by higher rainfall and antecedent wetness, I_G and SWC emerged
343 as more effective indicators for estimating the occurrence of bimodal events, while peak rainfall
344 intensity, mean rainfall intensity, and API were found to be insufficient for distinguishing between
345 bimodal and unimodal events.



346
 347 **Figure 4.** Box plots of the hydrological characteristic parameters for unimodal and bimodal events.
 348 (a) rainfall amount; (b) mean rainfall intensity; (c) peak rainfall intensity; (d) I_G : groundwater level
 349 index; (e) soil water content; (g)-(i) API3, API6 and API12: antecedent precipitation index over 3,
 350 6 and 12 days. UE, BE and HBE are respectively unimodal, bimodal and hybrid bimodal events.
 351 To be noted, each element of the box carries the same interpretation as described in Fig. 3.

352

353 Considering the interdependence of groundwater level, streamflow, and SWC on rainfall, a
 354 detailed examination of the relationship between rainfall amount and bimodal events was
 355 conducted. The analysis revealed that the occurrence of delayed peaks is contingent on both event
 356 rainfall and antecedent wetness, displaying a distinct threshold behavior (Fig. 5b). The combined
 357 sum of event rainfall amount (P) and antecedent soil moisture index prior to the rainfall (ASI_0)
 358 serves as a reliable indicator for predicting the occurrence of delayed peaks. Fig. 5 illustrates that
 359 bimodal events tend to manifest when $P + ASI_0$ exceeds 200 mm (with only two bimodal events
 360 misplaced). An intriguing observation is that these misplaced bimodal events produced very little
 361 q_s , and these unimodal events nearby to the threshold, occurred just before the year's first bimodal
 362 response when the watershed was sufficiently humid, signaling a predisposition for bimodal events.
 363 However, once the rainfall surpassed the threshold, all bimodal episodes were randomly
 364 distributed, and no discernible relationship was observed between their stormflow volume (q_s) and
 365 rainfall amount. Based on these findings, we posit that the stormflow generation process may be
 366 dominated by groundwater or SWC.



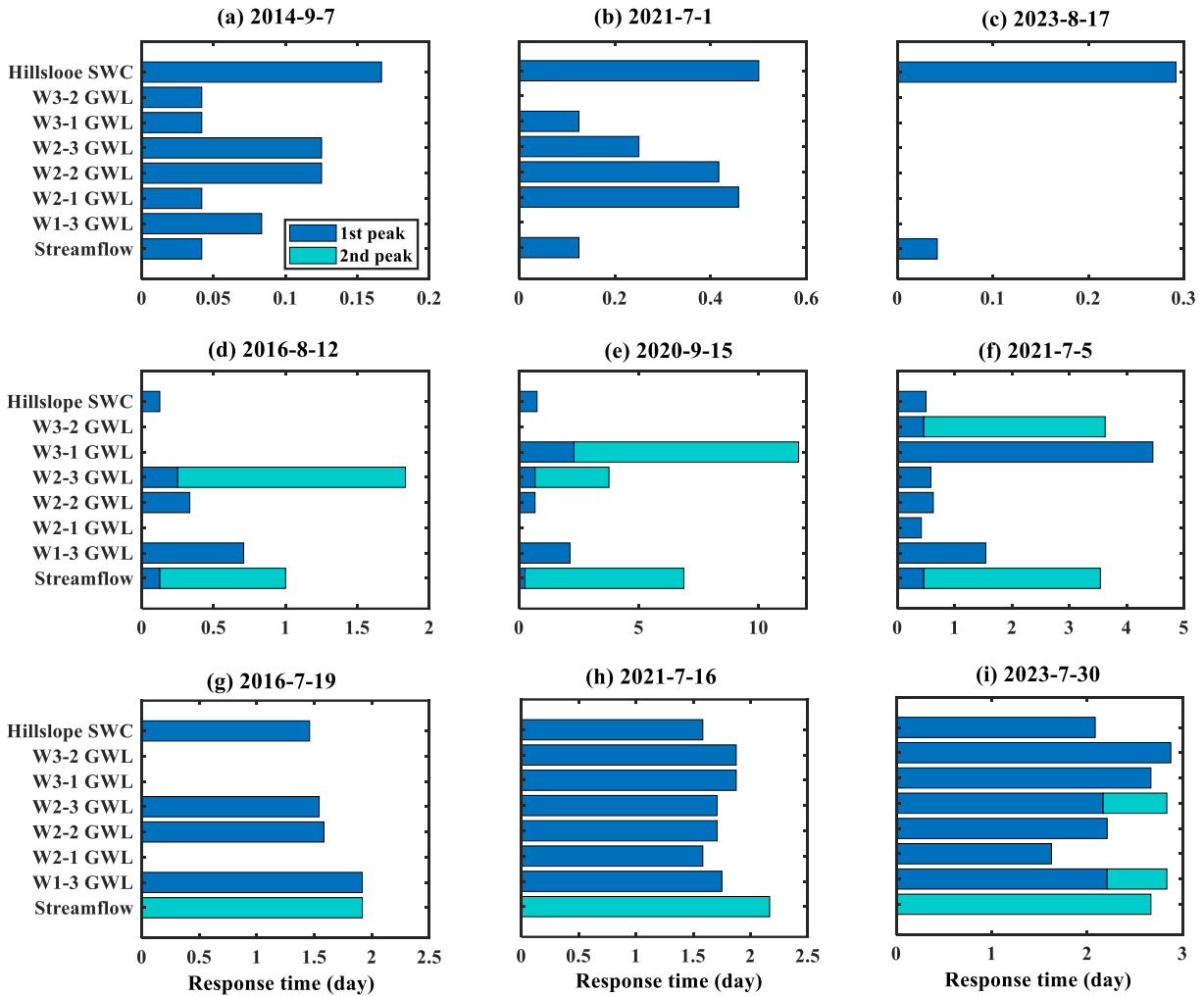
367
 368 **Figure 5.** Relationship between the $ASI_0 + P$ and stormflow volumes (q_s) of different event types.
 369 UE is unimodal event, HBE is hybrid bimodal event, P is rainfall amount, and ASI_0 is antecedent
 370 soil moisture index before the rainfall.

371

372 3.3 Timing of groundwater, soil water, and streamflow response

373 The preceding analysis indicates a correlation between different event types and groundwater
374 levels along with SWC. Moreover, the inconsistent response time among different event types may
375 signify distinct contributing sources to the stream channel, providing insights into the primary
376 mechanisms behind runoff generation. Earlier or identical response timing of groundwater
377 compared with streamflow suggested that streamflow response was driven by hillslope
378 groundwater (Haught and Meerveld, 2011; Rinderer *et al.*, 2016). To explore this further, six
379 bimodal events with minimal or sporadic rainfall during the delayed peak period, along with three
380 unimodal events, were selected. The response timing of groundwater, SWC, and streamflow is
381 illustrated in Fig. 6. Each horizontal bar represents the onset of rain on the left end and the lag time
382 for the peak value on the right end of the corresponding variable. It's worth noting that some
383 groundwater levels in Fig. 6d, e, and g lack horizontal bars due to missing groundwater level data,
384 while the groundwater levels in Fig. 6c lack horizontal bars due to no response from groundwater.

385 SWC reached their maximum after direct streamflow peaks but before delayed peaks.
386 Particularly in typical bimodal events, SWCs peaked much earlier than delayed streamflow peaks,
387 suggesting that, in these events, soil water did not contribute to direct peak but may to delayed
388 streamflow peaks. Regarding groundwater levels, some locations showed two peaks and not all
389 responded to the same rainfall event. Among different locations, groundwater levels peaked before
390 or after the delayed streamflow peaks. However, for the hybrid bimodal events, the response time
391 of groundwater levels at various locations, and even the SWC tended to coincide with the delayed
392 streamflow peak. Identical response timing or groundwater rising and peaking just before the
393 stream suggest that whole catchment or critical zone contributed to delayed stormflow.



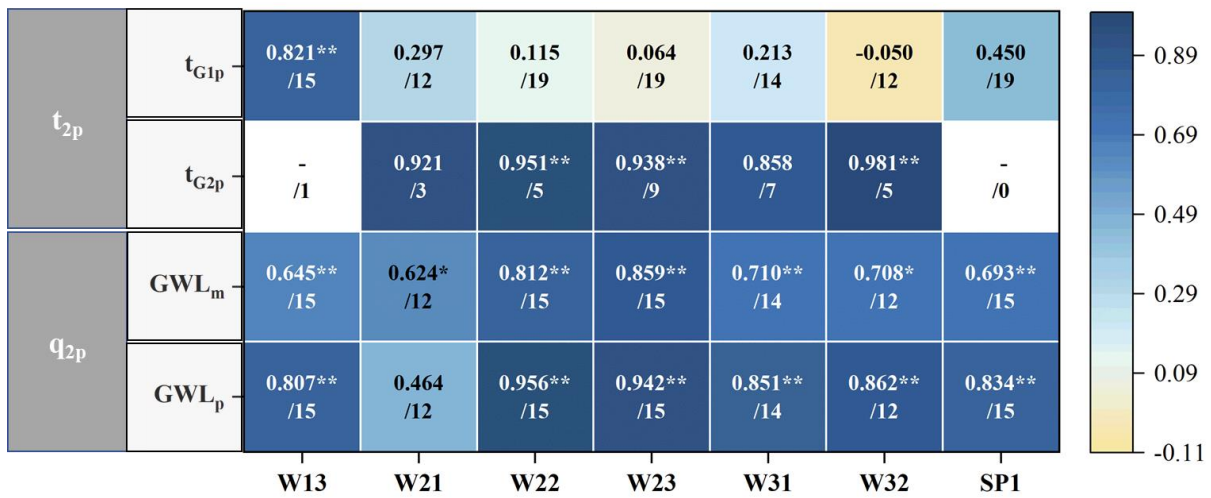
394

395 **Figure 6.** Response time of streamflow, groundwater level and soil water content in nine events.
 396 The horizontal axis illustrates the lag time from the onset of rainfall. The bar lengths depict the
 397 time taken for volumetric water content and groundwater level to reach their respective maximums
 398 from the onset of rainfall. GWL is groundwater level, and SWC is soil water content. Each row
 399 and column chart shares identical vertical and horizontal axis titles.

400 Pearson correlation coefficients (r_p) between peak groundwater levels, peak SWC and
 401 delayed streamflow were calculated for 19 bimodal events. As showed in Fig. 7, the first two lines
 402 show the correlation coefficients between t_{2p} and the lag time of the peak groundwater levels and
 403 SWC, t_{G1p} and t_{G2p} represent the response times of the first and second peaks of groundwater level
 404 or SWC, respectively. The last two lines show the correlation coefficients between q_{2p} and the

405 average and peak values of groundwater levels and SWC. The number after the slash specifies
 406 how many pairs of the variables.

407 Groundwater levels exhibited two peaks in some events, with the exception of W13.
 408 Correspondingly, among these events, the response time of the second peak of groundwater level
 409 has a strong correlation with t_{2p} with the $r_p > 0.858$. Even though W13's groundwater level only
 410 has one peak, this peak's response time was highly correlated with t_{2p} at the 0.01 significance level
 411 ($r_p = 0.821$). In contrast, SWC displayed one peak in all events, and its response time exhibited a
 412 weak correlation with t_{2p} ($r_p = 0.450$). Both groundwater levels and SWC, particularly their peak
 413 values, demonstrated a high correlation with delayed stormflow volumes (q_s). Above all,
 414 groundwater is deemed to be the primary controlling factor in delayed stormflow.



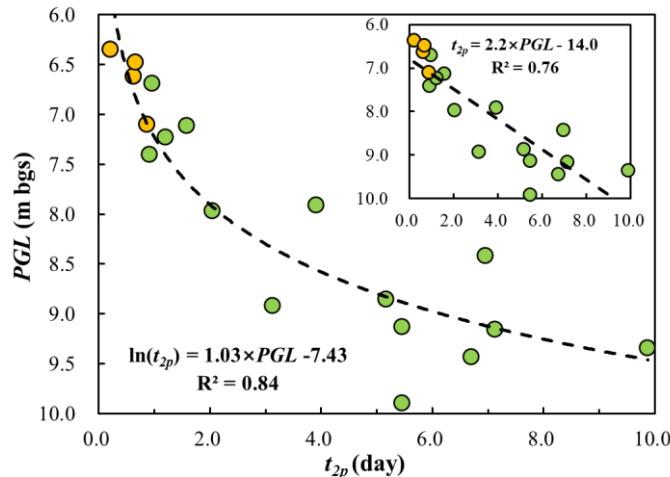
415
 416 **Figure 7.** Pearson correlation coefficients between peak streamflow and peak groundwater levels.
 417 The number after the slash specifies how many pairs of the variables. I_G , groundwater water level
 418 index; ** Denotes that correlation is significant at the 0.01 level (two-tailed).
 419

420 The robust correlation observed between groundwater levels at different locations and
 421 stormflow suggests that groundwater observations at a specific location can serve as a
 422 representative proxy for the overall groundwater level across the watershed. Given the relatively

423 complete and dynamic water level observation data for W23, this borehole was selected for further
424 analysis.

425 3.4 Stormflow timing and magnitude characteristics

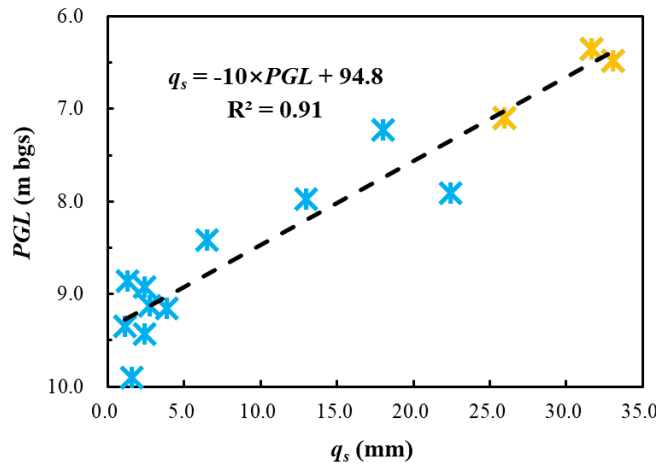
426 Considering the high correlation between streamflow and groundwater level as indicated in
427 the previous analysis, we hypothesized a connection between groundwater and delayed stormflow.
428 To elucidate this correlation between groundwater and streamflow, we fitted the relationship
429 between the groundwater level at location W23 and the magnitude and timing of the delayed
430 stormflow for bimodal events. The time lag of delayed peak (t_{2p}) shows a negative exponential
431 correlation with peak groundwater level ($\ln(t_{2p}) = 1.03 \times PGL - 7.43$, $R^2 = 0.84$, $p < 0.01$, Fig. 8),
432 suggesting that a higher groundwater level corresponds to a faster response of the delayed runoff
433 peak to rainfall. A comparable linear correlation was also fitted between t_{2p} and groundwater level,
434 albeit with a slightly lower R^2 ($R^2 = 0.76$).



435 **Figure 8.** Correlation between peak groundwater level (PGL) and lag time of the delayed
436 streamflow peak (t_{2p}). The insert shows the same plot with linear fitting. Orange solid circles
437 represent hybrid bimodal events.
438

439 Moreover, as shown in Fig. 9, q_s also has a strong linear relationship with groundwater level
440 ($q_s = -10 \times PGL + 94.8$, $R^2 = 0.91$, $p < 0.01$). These results highlight the significant influence of

441 groundwater on flood generation in the studied watershed, suggesting that incorporating
442 groundwater level variations into flood forecasting models could enhance their accuracy.



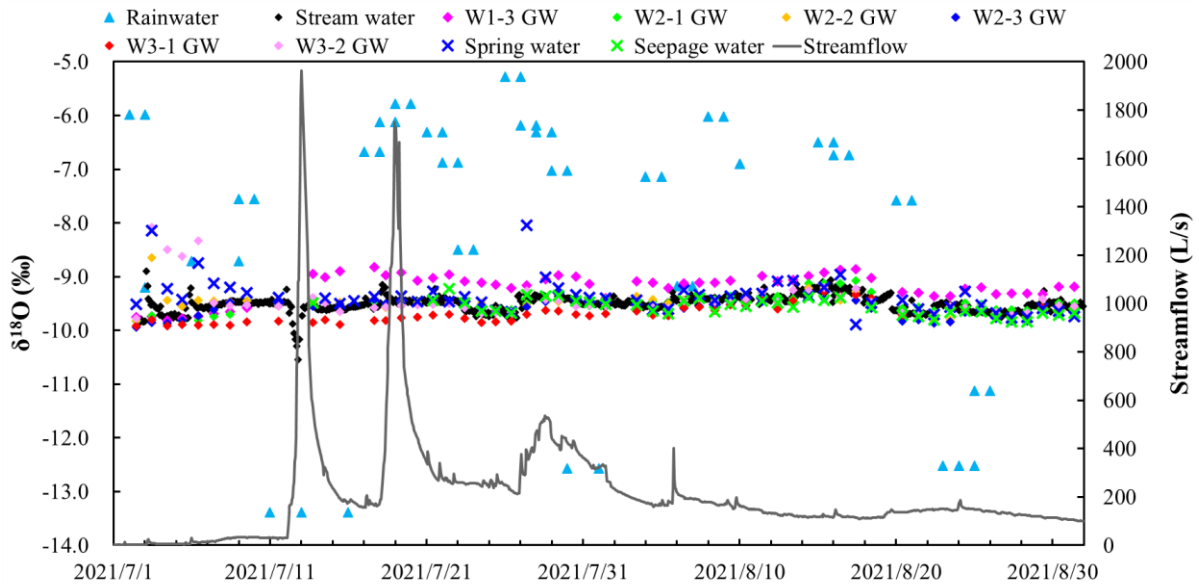
443
444 **Figure 9.** Correlation between peak groundwater (*PGL*) level and stormflow amount (*qs*) for
445 bimodal events. Orange stars represent hybrid bimodal events.

446 For both fitted lines, the closely matching fitting lines for hybrid bimodal events support the
447 hypothesis that these high, delayed streamflow responses, which may appear unimodal, are, in fact,
448 bimodal. During hybrid bimodal events, the delayed peak increased rapidly and reached its peak
449 within one day, practically merging with the direct peak. This led to a potentially misleading result
450 that only one peak was generated. This occurrence was likely due to the groundwater level rising
451 rapidly to a critical level with substantially higher hydraulic conductivity, allowing a larger portion
452 of the hillslope to become hydraulically connected to the stream during these events within a very
453 short time. Consequently, a substantial amount of groundwater was quickly discharged into the
454 channel.

455 3.5 Isotope composition of groundwater and stream water

456 To gain additional insight into the control of groundwater level on delayed stormflow, the
457 isotope compositions of different water bodies were analyzed. Fig. 10 summarizes the $\delta^{18}\text{O}$ of
458 stream, spring, seepage water and the groundwater $\delta^{18}\text{O}$ from all boreholes between July 1 and

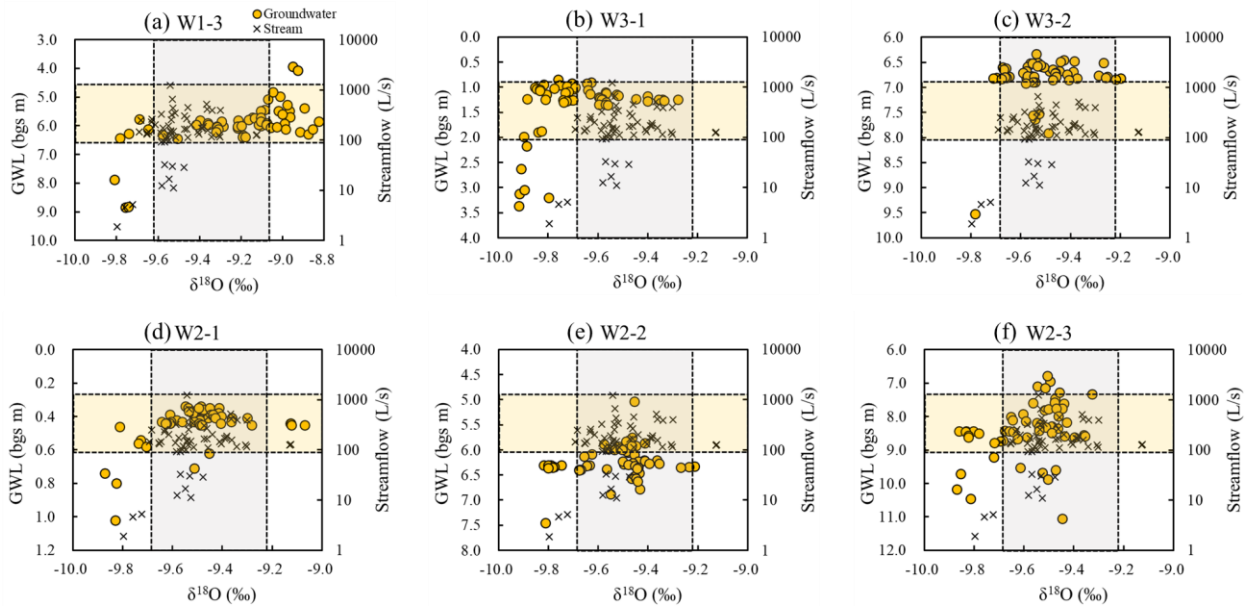
459 September 1 in 2021. Rainwater exhibited a high variation in $\delta^{18}\text{O}$ composition (ranging from -
 460 14.42 to -5.28 ‰), with a rainfall-weighted mean $\delta^{18}\text{O}$ value of -9.197. In contrast, groundwater
 461 $\delta^{18}\text{O}$ composition appeared more stable throughout the sampling period, showing little variation
 462 across various boreholes, with a mean $\delta^{18}\text{O}$ value ranging from -9.76 ± 0.10 to -9.08 ± 0.86 ‰. This
 463 stability indicates minimal event-based mixing with rainwater. The $\delta^{18}\text{O}$ values of spring and
 464 seepage water followed a pattern similar to that of groundwater. The average $\delta^{18}\text{O}$ value of the
 465 stream (-9.51‰) closely resembled that of groundwater (-9.49‰). Although the stream's $\delta^{18}\text{O}$
 466 composition briefly deviated toward that of rainfall during a storm, it quickly reverted to its
 467 previous value, resembling groundwater. Large isotopic variation in rainfall was dampened in the
 468 stream, indicating that both baseflow and some stormflow originated from groundwater storage
 469 with a consistent isotopic ratio, a result of dispersion and mixing processes.



470 **Figure 10.** Stable isotope $\delta^{18}\text{O}$ time series of rainwater, stream water and groundwater.
 471

472 In Fig. 11, groundwater $\delta^{18}\text{O}$ values were plotted against groundwater levels for each
 473 borehole, and stream water $\delta^{18}\text{O}$ values were plotted against streamflow. The variability of
 474 groundwater $\delta^{18}\text{O}$ increased with rising groundwater levels, suggesting a stronger influence of

475 rainwater on groundwater. Stream water's $\delta^{18}\text{O}$ remained independent of streamflow volume and
 476 exhibited a range of variation similar to that of groundwater. Notably, the overlapping isotopic
 477 compositions, including those during stormflow, were predominantly found in regions with higher
 478 groundwater levels. This observation underscores that, even during stormflow events, groundwater
 479 remains the primary source of streamflow.



480
 481 **Figure 11.** $\delta^{18}\text{O}$ measurements in groundwater and stream water from July 1 to September 1, 2021.
 482 Circles and cross represent the $\delta^{18}\text{O}$ of groundwater and stream water, respectively.

483 **4. Discussion**

484 **4.1 Lag time of delayed streamflow peaks**

485 The lag time of delayed peaks varies across different water sources, providing valuable
 486 insights for estimating stormflow water resources. Haga *et al.* (2005) conducted relevant studies
 487 in a forested unchanneled catchment, noting that events with shorter lag times (<2 hours)
 488 predominantly exhibited runoff composed of saturation excess overland flow near the spring area.
 489 In contrast, events with longer lag times (>24 hours) were characterized by river runoff mainly

490 composed of saturated subsurface flow above the soil-bedrock interface. Becker (2005)
491 synthesized lag times from various studies in different basins, observing a trend where lag times
492 for the three main flow components differed by at least one order of magnitude, following the
493 pattern overland flow < subsurface flow < baseflow. This substantial difference in lag times is
494 likely attributed to the stochastic triggering of different flow paths by rainfall forcing in distinct
495 events.

496 Lag times for the direct streamflow peaks, observed in both unimodal and bimodal events in
497 this study, were generally within 30 minutes. These lag times exhibited no significant correlation
498 with rainfall amount, rainfall intensity, or pre-event streamflow (correlation coefficients of 0.005,
499 0.017, and 0.012, respectively). This lack of correlation suggests that the direct streamflow peaks
500 were nearly concurrent with rainfall. Therefore, we infer that these direct peaks were generated
501 either through bypass flow mechanisms, such as macropores, fractures, or soil-bedrock interfaces,
502 as interpreted in Buttle and Turcotte (1999), Onda *et al.* (2001), Uchida *et al.* (2005), and Xu *et al.*
503 (2016). Alternatively, they could have been directly contributed to the channel by rainfall. This
504 interpretation aligns with the consideration that the routing time of the river network in XEW is
505 approximately 1 hour (Zhao *et al.*, 2019).

506 In contrast to the direct peaks, the time lags from the peak rainfalls to the delayed peaks were
507 considerably longer, ranging from 5 hours to 9.9 days (Fig. 3). This lag time in our study aligns
508 with findings from other studies where similar parameters were calculated (refer to Table 3). The
509 results imply that the delayed peaks observed in XEW were likely generated by subsurface flow
510 processes, as indicated in the work of Lischeid *et al.* (2002).

511

512

513 **Table 3.** Lag time between peak rainfall intensity and the delayed streamflow peak in this study
 514 and in previous studies.

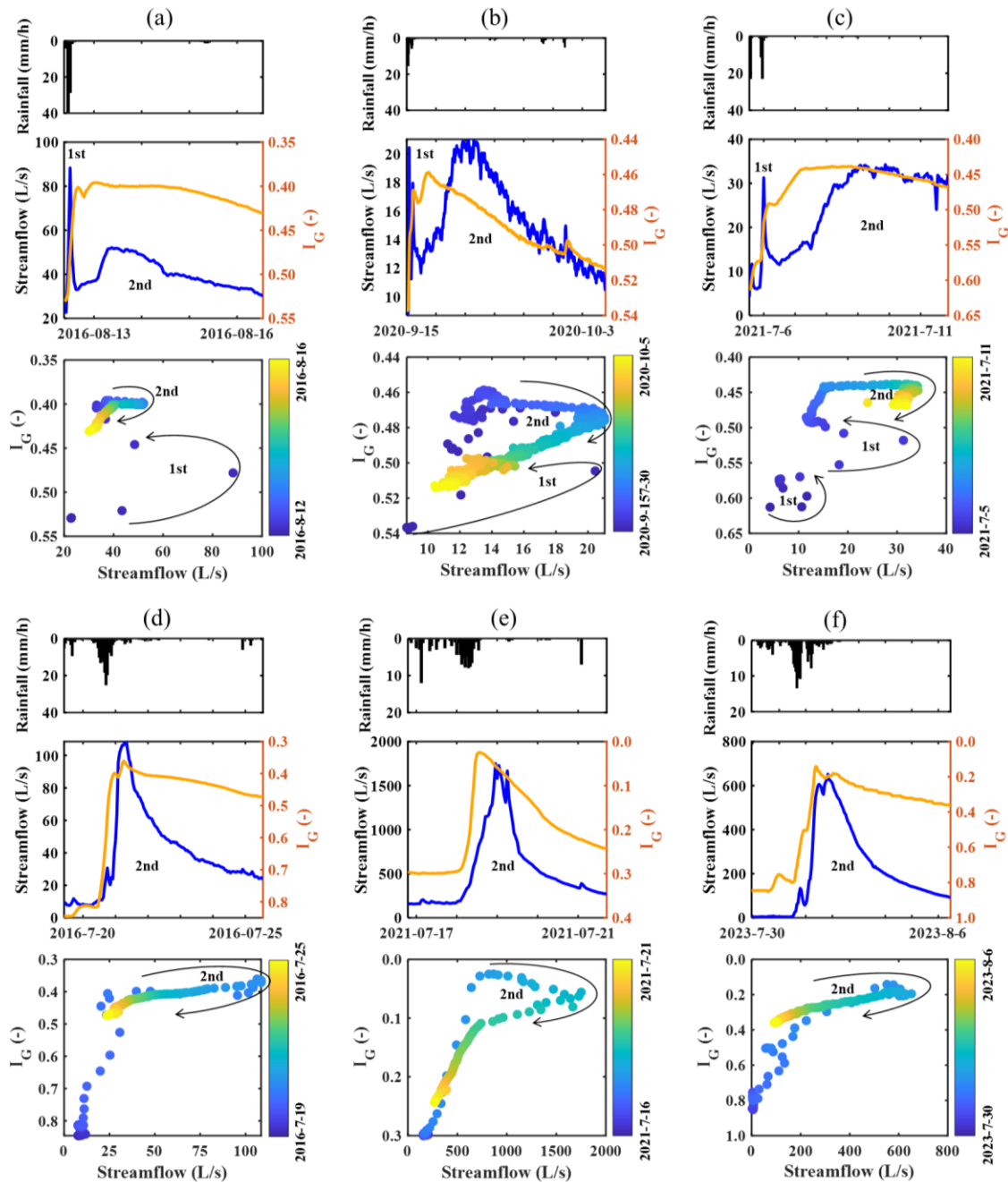
Reference	Lag time of delayed peak	The source of the delayed peak
Anderson & Burt (1978)	About one day	Subsurface flow
Onda <i>et al.</i> (2001)	Ten hours to one week	Subsurface flow and bedrock groundwater
Masiyandima <i>et al.</i> (2003)	Several hours	Subsurface flow
Becker (2005)	A day to several weeks	Subsurface stormflow
Zillgens <i>et al.</i> (2007)	Three to five days	Subsurface flow
Birkinshaw (2008)	Several tens of hours to a few days	Subsurface stormflow
Kosugi <i>et al.</i> (2011)	Two to three days	Bedrock groundwater
Fenicia <i>et al.</i> (2014)	Several hours or days	Subsurface flow
Padilla <i>et al.</i> (2014, 2015)	Within four days	Bedrock groundwater
Yang <i>et al.</i> (2015)	Several hours	Subsurface flow
This study	5 hours to 9.9 days	Subsurface flow (groundwater flow)

515

516 **4.2 Hysteresis between groundwater level and streamflow**

517 For bimodal events in XEW, the non-linear relationship between groundwater level and
 518 streamflow results in hysteretic relationships between the two variables. Fig. 12 shows time series
 519 for streamflow and I_G as well as scatter plots comparing the two variables for the six events used
 520 in section 3.3. As noted by Dunne (1978), when two runoff peaks appeared in an event, there must
 521 be at least two zones in the catchment that responded to the storm and contributed to runoff. The
 522 hysteretic nature highlights the possibility of multiple hydrological compartments being active and

523 these compartments are not necessarily contributing significant flows simultaneously but rather
 524 sequentially during the runoff generation period (Fovet *et al.*, 2015; Martínez-Carreras *et al.*, 2016).



525
 526 **Figure 12.** Streamflow and I_G with corresponding scatter plots between both variables for three
 527 typical bimodal and three hybrid bimodal events. Note that the axis scales vary between events.
 528 Arrows indicate progression of time. Direct peaks in bimodal hydrographs indicated as “1st” and
 529 delayed peaks as “2nd”.

530

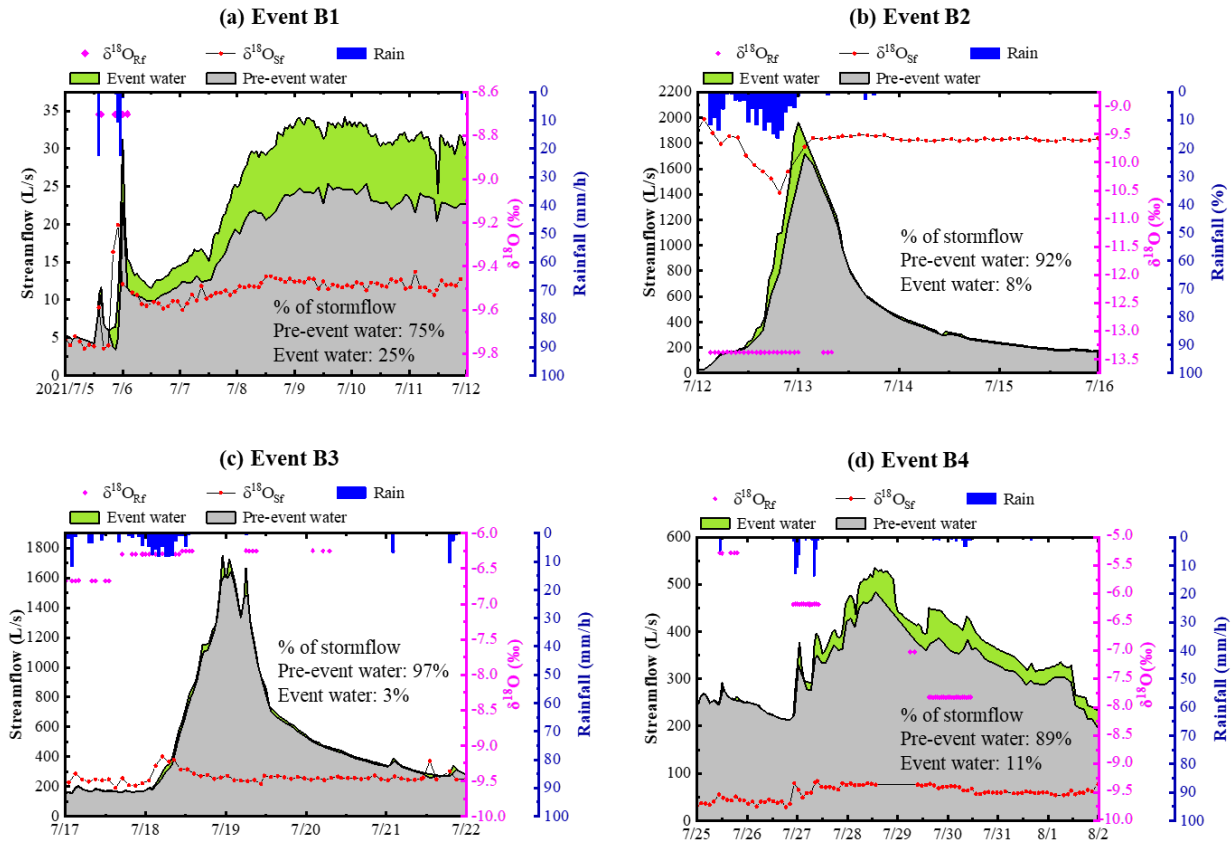
531 Streamflow increased quickly and peaked before groundwater level during direct peaks,
532 resulting in an anti-clockwise hysteretic loop. It can be explained that direct peaks were formed by
533 rainfall directly falling onto the channel or a saturation zone near the channel, and/or by the flow
534 that contributed to the channel through rapid routes, as observed in other watersheds by Jackisch
535 *et al.* (2016). In contrast, groundwater level peaked first during delayed peaks, indicating that the
536 groundwater level in the watershed peaked first and subsequently released water, creating the
537 delayed runoff peak. This behavior may be attributed to the groundwater level surpassing a
538 threshold for generating bimodal hydrographs, leading to enhanced hydraulic connectivity
539 between hillslopes and the channel. This, in turn, resulted in the swift release of a substantial
540 amount of groundwater or subsurface flow (Burt & Butcher, 1985; Detty and McGuire, 2010;
541 McGlynn & McDonnell, 2003; McGuire and McDonnell, 2010; Scaife and Band, 2017).
542 Consequently, the groundwater level is not merely a passive feature in this watershed, where
543 shallow groundwater may constitute the primary runoff component, but actively controls the
544 stormflow.

545 **4.3 Two-component hydrograph separation**

546 The two-component hydrograph separation was performed for four bimodal storm events
547 using the $\delta^{18}\text{O}$ of the bulk rainfall, a pre-event water signature (represented by the stream $\delta^{18}\text{O}$
548 before the rainfall) and the monitored stream water signature during the events. These four events
549 were chosen because their relatively complete isotope data. It should be noted that in all four
550 rainfall events, $\delta^{18}\text{O}$ values in rain and stream water were notably different, which is a requirement
551 for end-member hydrograph separation analysis. The hydrograph separation results, as well as the
552 $\delta^{18}\text{O}$ series of rainwater and stream water were shown in Fig. 13.

553 Regarding the water sources separation result, these four events can be divided into two
554 groups: Event B1 and B4, the major stormflow process were lagged and considerably damped, and
555 event water contributions were higher compared to the other two events. The fraction of event
556 water comprising the hydrograph was 25% in Event B1, and the contribution ratio of event water
557 in Event 4 was 11%. Considering that the rain had already stopped, the event water component of
558 the delayed peak should be the rainwater temporarily stored in the watershed during the rainfall
559 process. Event B2 and especially Event B3, however, were almost entirely pre-event water
560 dominated (the contributions of pre-event water were 92% for Event 2 and 97% for Event B3),
561 although it was evident that some event water contributed to the stormflow during the rising and
562 peak period of streamflow, this water may have originated from the direct rainfall or rain water
563 taking a rapid route to the stream channel.

564 The hydrograph separation results indicated that the streamflow contribution of pre-event
565 water changed virtually in sync with streamflow following the onset of rain, almost entirely
566 dominating the hydrograph, while event water dominated the sharp streamflow peak responding
567 to high-intensity storm. Early in the rainy event, the pre-event component of the hydrograph
568 exceeded 50%, indicating a sufficiently swift groundwater response such that considerable
569 amounts of groundwater were released soon after the start of rain.



570
 571 **Figure 13.** The partitioning of stormflow into its pre-event and event water sources using one-
 572 tracer two component hydrograph separation analysis with $\delta^{18}\text{O}$ as tracer for the four storm
 573 events. $\delta^{18}\text{O}_{\text{Rf}}$ and $\delta^{18}\text{O}_{\text{Sf}}$ are the $\delta^{18}\text{O}$ respectively for rain and stream water.

574 In addition, there was a noticeable, gradual rise in the pre-event water contribution to total
 575 stormflow as the catchment was wetting-up (Fig. 13). Event B1 had a rather dry antecedent
 576 condition and showed a relatively lower pre-event water percentage (about 75%). Event 3 in the
 577 temporal sequence had a extremely high pre-event water proportion (approximately 97%) and
 578 occurred under highly wet antecedent conditions. In Event B4, due to a little reduced wetness
 579 condition compared to the preceding Event B3, the percentage of pre-event water decreased
 580 somewhat to approximately 89%. This pattern may be attributed to increased water flux during the
 581 wetting-up process when the water table rose into near surface soil layers with high saturated
 582 hydraulic conductivity. The rate of groundwater increase slowed as a result of the higher

583 transmissivity, and more pre-event water was mobilized and travelled rapidly to the stream via
584 shallow flow pathways (Lundin, 1982).

585 4.4 Field observation

586 Our field observations on-site indicate that direct exfiltration of groundwater into the runoff
587 predominates, with few signs of hillslope overland flow. For example, during a heavy storm on
588 July 5, 2021, characterized by short duration (7 hours) and very high intensity (27.6 mm/h) with a
589 total rainfall of 65.2 mm, minimal overland flow was observed at the study site. However, post the
590 storm on July 5, the spring water flow from Hillslope 2 substantially increased. Moreover, at
591 various points in the watershed, seepage flow was observed gushing from fractures in the stone
592 and holes in the earth. These field observations strongly suggest the direct exfiltration of
593 groundwater into the runoff, providing further support to the notion that groundwater significantly
594 contributes to stormflow in the watershed.



595
596 **Figure 14.** Field observations of the spring and the seepage flows. HS1, HS2 and HS3 are Hillslope
597 1, Hillslope 2 and Hillslope 3, respectively.

598 5. Conclusions

599 Based on observations from 2013 to 2023, the study carried out an event-scale analysis of
600 streamflow hydrographs in a semi-humid forested watershed of North China. Three stormflow

601 patterns with distinct shaped hydrograph, i.e., unimodal, bimodal, and hybrid bimodal were
602 identified. Particularly, their rainfall-runoff response characteristics as well the stormflow
603 composition were analyzed, and derived the following conclusions:

604 1) Direct peaks for both unimodal and bimodal events occurred within 1 hour following the
605 peak rainfall, while the lag time of delayed peaks ranged between 5 h and 9.9 days. The stormflow
606 amount generated by bimodal events, due to the delayed peak, was several to hundreds of times
607 more than that of the unimodal events, often resulting in flooding.

608 2) Delayed stormflow appeared when the sum of event rainfall amount (P) and antecedent
609 soil moisture index (ASI) exceeding 200 mm. Stormflow yield is positively proportional to event
610 peak groundwater level while the lag time of delayed peak showed an inverse correlation with
611 peak groundwater level.

612 3) The isotopic analysis and two-component hydrograph separation unveiled that pre-event
613 water predominantly contributed to the delayed stormflow, with event water dominating the sharp
614 streamflow peak in response to high-intensity storms.

615 4) Streamflow peaked before groundwater level during direct peaks, suggesting that direct
616 streamflow peaks are from direct rainfall onto the channel or rapid flow through macropores and
617 bedrock fractures, Discharge peaked before catchment storage during single peak. But
618 groundwater levels peaked first during delayed streamflow, suggested that the delayed stormflow
619 is primarily made up of shallow groundwater, and this is further supported by field observation.

620 This study clarified the prerequisites for bimodal stormflow, and the provided information on
621 the response characteristics and water resources of stormflow is not common knowledge for
622 regions. We believe these findings can enrich runoff generation theory and contribute new insights
623 for stormflow modelling in other similar regions.

624 **Data availability**

625 The data supporting this study are available on the Zenodo website at
626 <https://doi.org/10.5281/zenodo.12581739>.

627 **Author contribution**

628 ZC contributed the conceptualization, formal analysis, investigation and writing; FT
629 contributed the conceptualization, formal analysis and revision; ZZ, ZX, YD and JW contributed
630 the Investigation; M contributed the writing.

631 **Competing interests**

632 Some authors are members of the editorial board of Hydrology and Earth System Sciences.
633 The peer-review process was guided by an independent editor, and the authors have also no other
634 competing interests to declare.

635 **Disclaimer**

636 Publisher's note: Copernicus Publications remains neutral with regard to jurisdictional claims
637 made in the text, published maps, institutional affiliations, or any other geographical representation
638 in this paper. While Copernicus Publications makes every effort to include appropriate place
639 names, the final responsibility lies with the authors.

640 **Financial support**

641 This study was supported by the National Natural Science Foundation of China (51825902)
642 and the National Key R&D Program of China (2022YFC3002902).

643 **Acknowledgments**

644 We would like to thank Jeffrey McDonnell for his constructive advice on this study.
645 Additionally, we are grateful to the two anonymous reviewers for their valuable feedback during
646 the revision process.

647 **References**

- 648 Ali, G., Tetzlaff, D., McDonnell, J. J., Soulsby, C., Carey, S., Laudon, H., McGuire, K., Buttle, J., Seibert, J.,
649 and Shanley, J.: Comparison of threshold hydrologic response across northern catchments, *Hydrol. Process.*,
650 29, 3575–3591, <https://doi.org/10.1002/hyp.10527>, 2015.
- 651 Anderson, M. G., and Burt, T. P.: Automatic monitoring of soil moisture conditions in a hillslope spur and
652 hollow, *J. Hydrol.*, 33, 0–36, [https://doi.org/10.1016/0022-1694\(77\)90096-8](https://doi.org/10.1016/0022-1694(77)90096-8), 1977.
- 653 Anderson, M. G., and Burt, T. R.: The role of topography in controlling throughflow generation, *Earth Surf.*
654 *Process.*, 3, 331–334, <https://doi.org/10.1002/esp.3290030402>, 1978.
- 655 Becker, A.: Runoff Processes in Mountain Headwater Catchments: Recent Understanding and Research
656 Challenges, in: *Global Change and Mountain Regions*, 283–295, [https://doi.org/10.1007/1-4020-3508-](https://doi.org/10.1007/1-4020-3508-x_29)
657 [x_29](https://doi.org/10.1007/1-4020-3508-x_29), 2005.
- 658 Becker, A., and McDonnell, J. J.: Topographical and ecological controls of runoff generation and lateral flows
659 in mountain catchments, *IAHS Publ.*, 248, 199-206, 1998.
- 660 Birkinshaw, S. J.: Physically - based modelling of double - peak discharge responses at Slapton Wood
661 catchment, *Hydrol. Process.*, 22, 1419–1430, <https://doi.org/10.1002/hyp.6694>, 2008.
- 662 Burt, T. P., and Butcher, D. P.: Topographic controls of soil moisture distributions, *J. Soil Sci.*, 36, 469–486,
663 <https://doi.org/10.1111/j.1365-2389.1985.tb00351.x>, 1985.
- 664 Buttle, J. M., Dillon, P. J., and Eerkes, G. R.: Hydrologic coupling of slopes, riparian zones and streams: An
665 example from the Canadian Shield, *J. Hydrol.*, 287, 161–177, <https://doi.org/10.1016/j.jhydrol.2003.09.022>,
666 2004.

667 Buttle, J. M., and Turcotte, D. S.: Runoff processes on a forested slope on the Canadian Shield, *Hydrol. Res.*,
668 30, 1-20, [https://doi.org/10.1016/S0304-2995\(99\)80027-8](https://doi.org/10.1016/S0304-2995(99)80027-8), 1999.

669 Detty, J. M., and Mcguire, R. J.: Threshold changes in storm runoff generation at a till-mantled headwater
670 catchment, *Water Resour. Res.*, 46, 759–768, <https://doi.org/10.1029/2009wr008102>, 2010.

671 Dingman, S. L.: *Physical hydrology*, Waveland Press, Long Grove, IL, 2015.

672 Dubreuil, P. L.: *Etude hydrologique de petits bassins en Cote d’Ivoire, Rapport general*, ORSTOM Service
673 Hydrologique, 1960.

674 Dubreuil, P. L.: Review of field observations of runoff generation in the tropics, *J. Hydrol.*, 80, 237–264,
675 [https://doi.org/10.1016/0022-1694\(85\)90119-2](https://doi.org/10.1016/0022-1694(85)90119-2), 1985.

676 Dunne, T.: Field studies of hillslope flow processes, in: *Hillslope Hydrology*, edited by: Kirkby, M. J., Wiley,
677 London, 227–293, 1978.

678 Fenicia, F., Kavetski, D., Savenije, H. H., Clark, M. P., Schoups, G., Pfister, L., and Freer, J.: Catchment
679 properties, function, and conceptual model representation: is there a correspondence?, *Hydrol. Process.*, 28,
680 2451–2467, <https://doi.org/10.1002/hyp.9726>, 2014.

681 Fovet, O., Ruiz, L., Hrachowitz, M., Faucheux, M., and Gascuel-Oudou, C.: Hydrological hysteresis and its
682 value for assessing process consistency in catchment conceptual models, *Hydrol. Earth Syst. Sci.*, 19, 105-
683 123, <https://doi.org/10.5194/hess-19-105-2015>, 2015.

684 Fu, C., Chen, J., Jiang, H., and Dong, L.: Threshold behavior in a fissured granitic catchment in southern China:
685 1. Analysis of field monitoring results, *Water Resour. Res.*, 49, 2519–2535,
686 <https://doi.org/10.1002/wrcr.20191>, 2013.

687 Graeff, T., Zehe, E., Reusser, D., Lück, E., Schröder, B., Wenk, G., John, H., and Bronstert, A.: Process
688 identification through rejection of model structures in a mid-mountainous rural catchment: observations of
689 rainfall-runoff response, geophysical conditions and model inter-comparison, *Hydrol. Process.*, 23, 702–
690 718, <https://doi.org/10.1002/hyp.7171>, 2009.

691 Gu, W.: On the hydrograph separation traced by environmental isotopes, *Adv. Water Sci.*, 7, 105–111, 1996.

692 Haga, H., Matsumoto, Y., Matsutani, J., Fujita, M., Nishida, K., and Sakamoto, Y.: Flow paths, rainfall properties,
693 and antecedent soil moisture controlling lags to peak discharge in a granitic unchanneled catchment, *Water*
694 *Resour. Res.*, 41, 2179–2187, <https://doi.org/10.1029/2005wr004236>, 2005.

695 Iwagami, S., Tsujimura, M., Onda, Y., Shimada, J., and Tanaka, T.: Role of bedrock groundwater in the rainfall-
696 runoff process in a small headwater catchment underlain by volcanic rock, *Hydrol. Process.*, 24, 2771–2783,
697 <https://doi.org/10.1002/hyp.7690>, 2010.

698 Jackisch, C., Angermann, L., Allroggen, N., Sprenger, M., Blume, T., Weiler, M., Tronicke, J., and Zehe, E.: In
699 situ investigation of rapid subsurface flow: identification of relevant spatial structures beyond heterogeneity,
700 *Hydrol. Earth Syst. Sci. Discuss.*, 1–32, <https://doi.org/10.5194/hess-2016-190>, 2016.

701

702 Jenkins, A., Ferrier, R. C., Harriman, R., and Ogunkoya, Y. O.: A case study in catchment hydrochemistry:
703 Conflicting interpretations from hydrological and chemical observations, *Hydrol. Process.*, 8, 335–349,
704 <https://doi.org/10.1002/hyp.3360080406>, 1994.

705 Kosugi, K., Fujimoto, M., Katsura, S., Kato, H., Sando, Y., and Mizuyama, T.: Localized bedrock aquifer
706 distribution explains discharge from a headwater catchment, *Water Resour. Res.*, 47,
707 <https://doi.org/1029/2010WR009884>, 2011.

708 Lischeid, G., Kolb, A., and Alewell, C.: Apparent translatory flow in groundwater recharge and runoff generation,
709 *J. Hydrol.*, 265, 195–211, [https://doi.org/10.1016/s0022-1694\(02\)00108-7](https://doi.org/10.1016/s0022-1694(02)00108-7), 2002.

710 Lundin, L.: Soil moisture and ground water in till soil and the significance of soil type for runoff, PhD Thesis,
711 Uppsala University, UNGI Report, 56, 216, 1982.

712 Martínez-Carreras, N., Hissler, C., Gourdol, L., Klaus, J., Juilleret, J., Iffly, J. F., and Pfister, L.: Storage controls
713 on the generation of double peak hydrographs in a forested headwater catchment, *J. Hydrol.*, 543, 255–269,
714 <https://doi.org/10.1016/j.jhydrol.2016.10.004>, 2016.

715 Martínez-Carreras, N., Wetzol, C. E., Frentress, J., Ector, L., McDonnell, J. J., Hoffmann, L., and Pfister, L.:
716 Hydrological connectivity inferred from diatom transport through the riparian-stream system, *Hydrol. Earth*
717 *Syst. Sci.*, 19, 3133–3151, <https://doi.org/10.5194/hess-19-3133-2015>, 2015.

718 Masiyandima, M. C., van de Giesen, N., Diatta, S., Windmeijer, P. N., and Steenhuis, T. S.: The hydrology of
719 inland valleys in the sub-humid zone of West Africa: rainfall-runoff processes in the M'be experimental
720 watershed, *Hydrol. Process.*, 17, 1213–1225, <https://doi.org/10.1002/hyp.1191>, 2003.

721 McDonnell, J. J., Bonell, M., Stewart, M. K., and Pearce, A. J.: Deuterium variations in storm rainfall:
722 Implications for stream hydrograph separation, *Water Resour. Res.*, 26, 455–458,
723 <https://doi.org/10.1029/WR026i003p00455>, 1990.

724 McDonnell, J. J., Sivapalan, M., Vaché, K., Dunn, S., Grant, G., Haggerty, R., Hinz, C., Hooper, R., Kirchner,
725 J., Roderick, M. L., Selker, J., and Weiler, M.: Moving beyond heterogeneity and process complexity: A
726 new vision for watershed hydrology, *Water Resour. Res.*, 43, <https://doi.org/10.1029/2006WR005467>,
727 2007.

728 McGlynn, B. L., and McDonnell, J. J.: Quantifying the relative contributions of riparian and hillslope zones to
729 catchment runoff, *Water Resour. Res.*, 39, 1310, <https://doi.org/10.1029/2003wr002091>, 2003.

730 McGuire, K. J., and McDonnell, J. J.: Hydrological connectivity of hillslopes and streams: Characteristic time
731 scales and nonlinearities, *Water Resour. Res.*, 46, <https://doi.org/10.1029/2010WR009341>, 2010.

732 Mosley, M. P.: Streamflow generation in a forested watershed, New Zealand, *Water Resour. Res.*, 15, 795–806,
733 <https://doi.org/10.1029/wr015i004p00795>, 1979.

734 Onda, Y., Komatsu, Y., Tsujimura, M., and Fujihara, J.: The role of subsurface runoff through bedrock on storm
735 flow generation, *Hydrol. Process.*, 15, 1693–1706, <https://doi.org/10.1002/hyp.234>, 2001.

736 Padilla, C., Onda, Y., Iida, T., Takahashi, S., and Uchida, T.: Characterization of the groundwater response to
737 rainfall on a hillslope with fractured bedrock by creep deformation and its implication for the generation of
738 deep-seated landslides on Mt. Wanitsuka, Kyushu Island, *Geomorphology*, 204, 444–458,
739 <https://doi.org/10.1016/j.geomorph.2013.08.024>, 2014.

740 Padilla, C., Onda, Y., and Iida, T.: Interaction between runoff-bedrock groundwater in a steep headwater
741 catchment underlain by sedimentary bedrock fractured by gravitational deformation, *Hydrol. Process.*, 29,
742 4398–4412, <https://doi.org/10.1002/hyp.10498>, 2015.

743 Penna, D., Tromp-van Meerveld, H. J., Gobbi, A., Borga, M., and Dalla Fontana, G.: The influence of soil
744 moisture on threshold runoff generation processes in an alpine headwater catchment, *Hydrol. Earth Syst.*
745 *Sci.*, 15, 689–702, <https://doi.org/10.5194/hess-15-689-2011>, 2011.

746 Phillips, J. D.: Sources of nonlinearity and complexity in geomorphic systems, *Prog. Phys. Geogr.*, 27, 1–23,
747 <https://doi.org/10.1191/0309133303pp340ra>, 2003.

748 Powell, D. N., Khan, A. A., Aziz, N. M., and Raiford, J. P.: Dimensionless rainfall patterns for South Carolina,
749 *J. Hydrol. Eng.*, 12, 130–133, [https://doi.org/10.1061/\(asce\)1084-0699\(2007\)12:1\(130\)](https://doi.org/10.1061/(asce)1084-0699(2007)12:1(130)), 2007.

750 Ross, C. A., Ali, G. A., Spence, C., and Courchesne, F.: Evaluating the Ubiquity of Thresholds in Rainfall-
751 Runoff Response Across Contrasting Environments, *Water Resour. Res.*, 57, e2020WR027498,
752 <https://doi.org/10.1029/2020wr027498>, 2021.

753 Scaife, C. I., and Band, L. E.: Nonstationarity in threshold response of stormflow in southern Appalachian
754 headwater catchments, *Water Resour. Res.*, 53, 6579–6596, <https://doi.org/10.1002/2017WR020376>, 2017.

755 Sivapalan, M.: Process complexity at hillslope scale, process simplicity at the watershed scale: Is there a
756 connection?, *Hydrol. Process.*, 17, 1037–1041, <https://doi.org/10.1002/hyp.5109>, 2003.

757 Sloto, R. A., and Crouse, M. Y.: HYSEP: A computer program for streamflow hydrograph separation and
758 analysis, *US Geol. Surv.*, <https://doi.org/10.3133/wri964040>, 1996.

759 Tian, F., Li, H., and Sivapalan, M.: Model diagnostic analysis of seasonal switching of runoff generation
760 mechanisms in the blue river basin, Oklahoma, *J. Hydrol.*, 418-419, 136–149,
761 <https://doi.org/10.1016/j.jhydrol.2010.03.011>, 2012.

762 Tie, Q., Hu, H., Tian, F., Guan, H., and Lin, H.: Environmental and physiological controls on sap flow in a
763 subhumid mountainous catchment in north China, *Agric. For. Meteorol.*, 240–241, 46–57,
764 <https://doi.org/10.1016/j.agrformet.2017.03.018>, 2017.

765 Tromp-van Meerveld, H. J., and McDonnell, J. J.: Threshold relations in subsurface stormflow: 1. A 147-storm
766 analysis of the Panola hillslope, *Water Resour. Res.*, 42, W02410, <https://doi.org/10.1029/2004WR003778>,
767 2006.

768 Uchida, T., Tromp-van Meerveld, I., and McDonnell, J. J.: The role of lateral pipe flow in hillslope runoff
769 response: An intercomparison of non-linear hillslope response, *J. Hydrol.*, 311, 117–133,
770 <https://doi.org/10.1016/j.jhydrol.2005.01.012>, 2005.

771 Westhoff, M. C., Bogaard, T. A., and Savenije, H. H. G.: Quantifying spatial and temporal discharge dynamics
772 of an event in a first order stream, using distributed temperature sensing, *Hydrol. Earth Syst. Sci.*, 15, 1945-
773 1957, <https://doi.org/10.5194/hess-15-1945-2011>, 2011.

774 Weyman, D. R.: Throughflow on hillslopes and its relation to the stream hydrograph, *Int. Assoc. Sci. Hydrol.*
775 *Bull.*, 15, 25–33, <https://doi.org/10.1080/02626667009493969>, 1970.

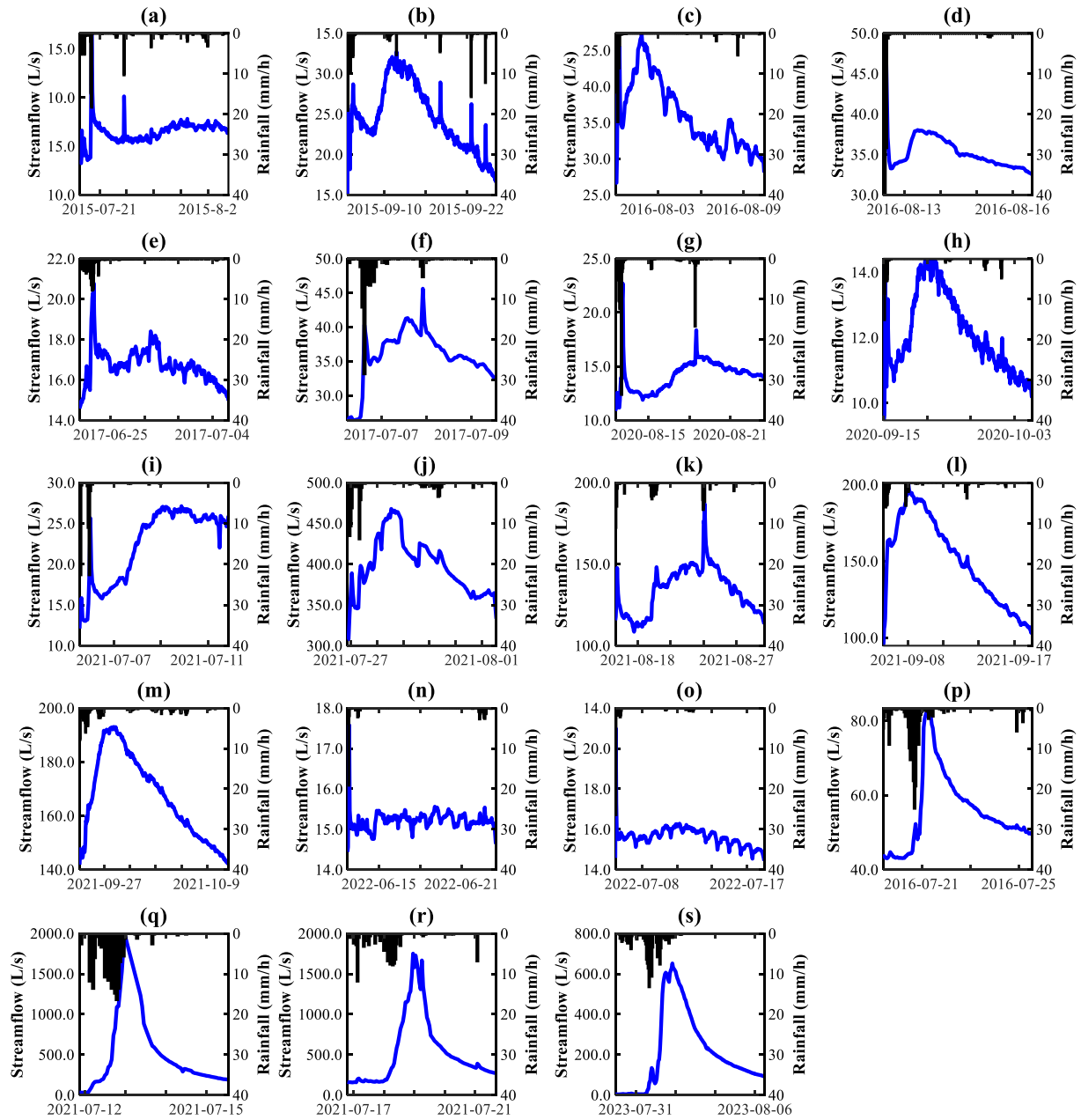
776 Wrede, S., Fenicia, F., Martínez-Carreras, N., Juilleret, J., Hissler, C., Krein, A., Savenije, H. H. G., Uhlenbrook,
777 S., Kavetski, D., and Pfister, L.: Towards more systematic perceptual model development: a case study
778 using 3 Luxembourgish catchments, *Hydrol. Process.*, 29, 2731–2750, <https://doi.org/10.1002/hyp.10393>,
779 2015.

780 Xu, Q., Liu, H., Ran, J., Li, W., and Sun, X.: Field monitoring of groundwater responses to heavy rainfalls and
781 the early warning of the Kualiangzi landslide in Sichuan Basin, southwestern China, *Landslides*, 13, 1555-
782 1570, <https://doi.org/10.1007/s10346-016-0717-3>, 2016.

783 Yang, Y., Endreny, T. A., and Nowak, D. J.: Simulating double-peak hydrographs from single storms over
784 mixed-use watersheds, *J. Hydrol. Eng.*, 20, 06015003, [https://doi.org/10.1061/\(ASCE\)HE.1943-](https://doi.org/10.1061/(ASCE)HE.1943-)
785 5584.0001225, 2015.

786 T., Wang, J., Tang, J. B., Chen, R., and Lei, M. Y.: Stormflow generation in a humid forest watershed controlled
787 by antecedent wetness and rainfall amounts, *J. Hydrol.*, 603, <https://doi.org/10.1016/j.jhydrol.2021.127107>,
788 2021.

789 Zillgens, B., Merz, B., Kirnbauer, R., and Tilch, N.: Analysis of the runoff response of an alpine catchment at
790 different scales, *Hydrol. Earth Syst. Sci.*, 11, 1441–1454, <https://doi.org/10.5194/hess-11-1441-2007>, 2007.
791



793
794 Figure A1. Rainfall and streamflow hydrograph for (a-o) 15 bimodal and (p-s) 4 hybrid bimodal
795 events.